Journal of Applied Analysis and Computation
Volume 9, Number 6, December 2019, 2224–2244
Website:http://jaac.ijournal.cn
DOI:10.11948/20190001

PATTERN FORMATION IN REACTION-DIFFUSION NEURAL NETWORKS WITH LEAKAGE DELAY*

Jiazhe Lin[1], Rui Xu[2,†] and Xiaohong Tian[2]

Abstract Due to the heterogeneity of the electromagnetic field in neural networks, the diffusion phenomenon of electrons exists inevitably. In this paper, we investigate pattern formation in a reaction-diffusion neural network with leakage delay. The existence of Hopf bifurcation, as well as the necessary and sufficient conditions for Turing instability, are studied by analyzing the corresponding characteristic equation. Based on the multiple-scale analysis, amplitude equations of the model are derived, which determine the selection and competition of Turing patterns. Numerical simulations are carried out to show the possible patterns and how these patterns evolve. In some cases, the stability performance of Turing patterns is weakened by leakage delay and synaptic transmission delay.

Keywords Pattern formation, reaction-diffusion, leakage delay, neural network, amplitude equation.

MSC(2010) 35K57, 35B32, 35B36, 35R10, 92B20.

1. Introduction

Over the past decades, neural networks and their various generalizations have attracted much attention in different fields of science and engineering, owing to their valuable applications in associative memory [1,3,18,26], pattern recognition [13,14], image processing [15,19] and so on. Early neural network models assumed that neurons respond synchronously to signals. In reality, time delay unavoidably occurs due to the finite speed of signal transmission and amplifiers switching, which is known as synaptic transmission delay. Usually, time delay is harmful to the dynamical behaviors of neural networks, causing oscillation, divergence, even chaos. In view of above-mentioned reasons, Olien and Bélair [16] proposed the following neural

†The corresponding author.
Email address: xurui@sxu.edu.cn or rxu88@163.com(R. Xu)
[1]Institute of Applied Mathematics, Army Engineering University, 050003 Shijiazhuang, China
[2]Complex Systems Research Center, Shanxi University, 030006 Taiyuan, China
*The authors were supported by the National Natural Science Foundation of China (Nos. 11871316, 11801340, 11371368) and the Natural Science Foundation of Shanxi Province (Nos. 201801D121006, 201801D221007).

network model with synaptic transmission delay

$$\begin{cases} \dfrac{du(t)}{dt} = -u(t) + a_1 f_1(v(t-\tau)) + b_1 g_1(u(t-\tau)), \\ \dfrac{dv(t)}{dt} = -v(t) + a_2 f_2(u(t-\tau)) + b_2 g_2(v(t-\tau)), \end{cases} \tag{1.1}$$

where $u(t), v(t)$ represent the voltage of different units; a_i, b_i $(i = 1, 2)$ denote connection weights; τ is the synaptic transmission delay; the transfer functions f_i, g_i $(i = 1, 2)$ are continuously differentiable, strictly increasing and odd. By linear stability analysis, Olien and Bélair found that Hopf bifurcation occurs when the delay passes through some critical values. Following this work, system (1.1) is further investigated by Huang etc [8,9]. Based on normal form method and center manifold theory, the direction of Hopf bifurcation and the stability of bifurcating periodic solution were obtained.

It is worth mentioning that the first term in each of the right side of system (1.1) corresponds to stabilizing negative feedback of the system which acts instantaneously without time delay and these terms are variously known as "forgetting" or leakage terms (see, for instance, [12]). In actual neural network circuits, when the neuron disconnects from the network connection and external input, it takes time to isolate to the static state. Gopalsamy [4,5] illustrated that this typical time delay in the negative feedback terms, which he called leakage delay, has a tendency to destabilize the system. There have been several works about the impact of leakage delay on neural networks (see, for example, [10,11]). In [11], Huang etc found that the leakage delay plays an important role in the dynamical behaviors of neural networks and may devastate the stability performance.

Besides, neural networks are realized by large scale integrated circuits, and the density of the electromagnetic field is generally not uniform. Therefore, in factual modeling, only considering the change of time seems to be not comprehensive when electrons are moving in asymmetric and nonuniform electromagnetic fields [20,21]. Influenced by diffusion, neural networks have rich spatial dynamical behaviors, like various Turing patterns. Spatial dynamics in reaction-diffusion systems was originally proposed by Turing [22] in 1952. This pioneering work of Turing not only came into being a theoretical foundation for understanding diverse patterns occurring in the natural world, but also opened a new research field, namely, pattern dynamics, which has received extensive attention and is still a hot topic in many scientific fields such as species dynamics [7,27,29], medicine [25,30], neural networks [2,23,28]. Based on the reaction-diffusion theory of Turing [22], Chua and Goraş [2] investigated the phenomenon of pattern formation in cellular neural networks. Recently, Zhao etc [28] proposed a model for reaction-diffusion neural network and obtained the conditions of Turing instability. By multiple-scale analysis method, the amplitude equations of the model are derived, which determine the stability of different spatial patterns. In [23], Tyagi etc investigated a general two-neuron delayed network model with reaction-diffusion terms and studied the existence of Hopf bifurcation and the conditions of Turing instability.

Motivated by Olien and Bélair [16], Gopalsamy [4] and Zhao etc [28], we are concerned with the effect of leakage delay on the pattern formation in reaction-diffusion neural networks. To this end, we consider the following reaction-diffusion

neural network with leakage delay and synaptic transmission delay

$$\begin{cases} \dfrac{\partial u(x,y,t)}{\partial t} = & d_1\Delta u(x,y,t) - c_1 u(x,y,t-\tau_1) + a_1 f_1(v(x,y,t-\tau_2)) \\ & + b_1 g_1(u(x,y,t)), \\ \dfrac{\partial v(x,y,t)}{\partial t} = & d_2\Delta v(x,y,t) - c_2 v(x,y,t-\tau_1) + a_2 f_2(u(x,y,t-\tau_2)) \\ & + b_2 g_2(v(x,y,t)), \end{cases} \tag{1.2}$$

under Neumann boundary condition

$$\frac{\partial u(x,y,t)}{\partial \mathbf{n}} = \frac{\partial v(x,y,t)}{\partial \mathbf{n}} = 0, \quad (x,y) \in \partial\Omega, \tag{1.3}$$

with initial condition

$$u(x,y,0) = u_0 > 0, \quad v(x,y,0) = v_0 > 0, \quad (x,y) \in \Omega, \tag{1.4}$$

where $u(x,y,t)$, $v(x,y,t)$ stand for state variables of neurons at time t and spatial position (x,y); a square domain $\Omega = (0,L)\times(0,L)$, in which L is a positive bounded constant; $\Delta = \frac{\partial^2}{\partial x^2} + \frac{\partial^2}{\partial y^2}$ is the Laplacian operator in two-dimensional space Ω; d_1 and d_2 are the diffusion coefficients of electrons between neurons; c_1 and c_2 describe the stability of internal neuron processes; τ_1 is leakage delay, while τ_2 is synaptic transmission delay; $\mathbf{n}$ is the outward unit normal vector of the boundary $\partial\Omega$ that is assumed to be smooth. Besides, c_1, c_2, d_1 and d_2 are positive constants.

System (1.2) is a fully connected single-layer neural network with self-feedback. Each neuron transmits its output to all the other neurons by connection weights and receives input from all the other neurons simultaneously. Thus, the output state of neuron in the network is indirectly related to its previous output state.

The paper is organized as follows. In Section 2, we analyze the linear stability of system (1.2) and obtain the conditions for the existence of Hopf bifurcation and the occurrence of Turing instability, respectively. In order to study the selection of Turing patterns, we use multiple-scale analysis to derive the amplitude equations of system (1.2) in Section 3. In Section 4, we investigate the stability of amplitude equations and construct different Turing patterns, which will be illustrated by numerical simulations in Section 5. In Section 6, the paper ends with a conclusion.

2. Linear stability analysis

Throughout this paper, we suppose that the following assumption holds.

(H1) f_j, $g_j \in C^{1,k}(\mathbb{R},\mathbb{R})$ $(j=1,2)$ with $k\geq 3$, which satisfy $f_j(0) = g_j(0) = 0$.

It is easy to show that if **(H1)** holds, system (1.2) always has a homogeneous steady state $E_0 = (u^0, v^0) = (0,0)$. In this section, we focus on the linear stability analysis of E_0. Linearizing system (1.2) at E_0 yields

$$\begin{cases} \dfrac{\partial u(x,y,t)}{\partial t} = d_1\Delta u(x,y,t) - c_1 u(x,y,t-\tau_1) + \phi_1 v(x,y,t-\tau_2) + \varphi_1 u(x,y,t), \\ \dfrac{\partial v(x,y,t)}{\partial t} = d_2\Delta v(x,y,t) - c_2 v(x,y,t-\tau_1) + \phi_2 u(x,y,t-\tau_2) + \varphi_2 v(x,y,t), \end{cases} \tag{2.1}$$

where $\phi_j = a_j f_j'(0)$, $\varphi_j = b_j g_j'(0)$ $(j = 1, 2)$. For simplicity, we assume that $\tau_1 = \tau_2 = \tau$. Expand the perturbation variables in the Fourier space

$$\begin{pmatrix} u \\ v \end{pmatrix} = \sum_{k=0}^{\infty} \begin{pmatrix} c_k^1 \\ c_k^2 \end{pmatrix} e^{\lambda_k t + \mathrm{i} k r}, \tag{2.2}$$

where λ_k is the growth rate of perturbations in time t, i is the imaginary unit and $\mathrm{i}^2 = -1$, $r = (x, y)$ is the spatial vector in two dimensions. Then substituting (2.2) into (2.1), the characteristic equation follows that

$$\lambda^2 + p_1\lambda + p_2 + (q_1\lambda + q_2)e^{-\tau\lambda} + re^{-2\tau\lambda} = 0, \tag{2.3}$$

where

$$\begin{aligned} &p_1 = k^2 d_1 + k^2 d_2 - \varphi_1 - \varphi_2, \quad p_2 = (k^2 d_1 - \varphi_1)(k^2 d_2 - \varphi_2), \\ &q_1 = c_1 + c_2, \quad q_2 = c_1(k^2 d_2 - \varphi_2) + c_2(k^2 d_1 - \varphi_1), \quad r = c_1 c_2 - \phi_1 \phi_2. \end{aligned}$$

2.1. Hopf bifurcation analysis

In this section, we investigate the existence of Hopf bifurcation in system (1.2). Firstly, multiplying $e^{\tau\lambda}$ on both sides of (2.3) yields

$$e^{\tau\lambda}\left(\lambda^2 + p_1\lambda + p_2\right) + (q_1\lambda + q_2) + re^{-\tau\lambda} = 0. \tag{2.4}$$

Substituting $\lambda = \mathrm{i}\omega$ into (2.4) and separating the real and imaginary parts yield

$$\begin{cases} (p_2 - \omega^2)\cos(\omega\tau) - p_1\omega\sin(\omega\tau) + q_2 + r\cos(\omega\tau) = 0, \\ (p_2 - \omega^2)\sin(\omega\tau) + p_1\omega\cos(\omega\tau) + q_1\omega - r\sin(\omega\tau) = 0. \end{cases} \tag{2.5}$$

Direct calculation shows that

$$\cos(\omega\tau) = -\frac{q_2(p_2 - \omega^2 - r) + p_1 q_1 \omega^2}{(p_2 - \omega^2)^2 - r^2 + p_1^2\omega^2}, \quad \sin(\omega\tau) = \frac{p_1 q_2 - q_1(p_2 - \omega^2 + r)}{(p_2 - \omega^2)^2 - r^2 + p_1^2\omega^2}\omega. \tag{2.6}$$

Noting that $\sin^2(\omega\tau) + \cos^2(\omega\tau) = 1$, ω is a positive real root of the following equation

$$\omega^8 + s_1\omega^6 + s_2\omega^4 + s_3\omega^2 + s_4 = 0, \tag{2.7}$$

where

$$\begin{aligned} s_1 &= 2p_1^2 - 4p_2 - q_1^2, \\ s_2 &= p_1^4 + 6p_2^2 + 2p_2 q_1^2 + 2q_1^2 r - 2r^2 - q_2^2 - 4p_1^2 p_2 - p_1^2 q_1^2, \\ s_3 &= 2p_1^2 p_2^2 + 4p_2 r^2 + 2p_2 q_2^2 + 4p_1 q_1 q_2 r - p_1^2 q_2^2 - 2p_1^2 r^2 - 4p_2^3 - 2q_2^2 r \\ &\quad - p_2^2 q_1^2 - q_1^2 r^2 - 2p_2 q_1^2 r, \\ s_4 &= p_2^4 + r^4 + 2p_2 q_2^2 r - 2p_2^2 r^2 - p_2^2 q_2^2 - q_2^2 r^2. \end{aligned}$$

From (2.6), we obtain that

$$\tau^{(n)} = \frac{1}{\omega}\left[\arccos\left(-\frac{q_2(p_2 - \omega^2 - r) + p_1 q_1 \omega^2}{(p_2 - \omega^2)^2 - r^2 + p_1^2\omega^2}\right) + 2n\pi\right],$$

in which $n = 0, 1, 2, \cdots$. Define $\tau_0 = \min\{\tau^{(n)}\}$. According to [17], Hopf bifurcation occurs when $\mathrm{Im}(\lambda_k) \neq 0$, $\mathrm{Re}(\lambda_k) = 0$, at $k = 0$. It is not difficult to obtain the following result.

Theorem 2.1. *For system* (1.2) *without diffusion, if Eq.* (2.7) *has at least one positive real root and* $\mathrm{Re}(\mathrm{d}\lambda/\mathrm{d}\tau)|_{\tau=\tau_0} \neq 0$*, the following results hold*

a) *The steady state* E_0 *is locally asymptotically stable for* $\tau \in [0, \tau_0)$*;*

b) *System* (1.2) *undergoes a Hopf bifurcation at the steady state* E_0 *when* $\tau = \tau_0$*, i.e., it has a branch of periodic solutions bifurcating from* E_0 *near* $\tau = \tau_0$*.*

In the following, we carry out some numerical simulations about Hopf bifurcation to support the theoretical analysis. By direct calculation, we obtain that $\omega = 2.2730$. In Fig. 1, we see that when $\tau = 0.02 < \tau_0 = 0.0759$, the steady state E_0 is locally asymptotically stable. As $\tau = 0.08 > \tau_0 = 0.0759$, Hopf bifurcation occurs in system (1.2). From Fig. 2, when τ varies from 0 to 0.15, the bifurcation diagram indicates that system (1.2) has rich and complex dynamics including chaotic behaviors.

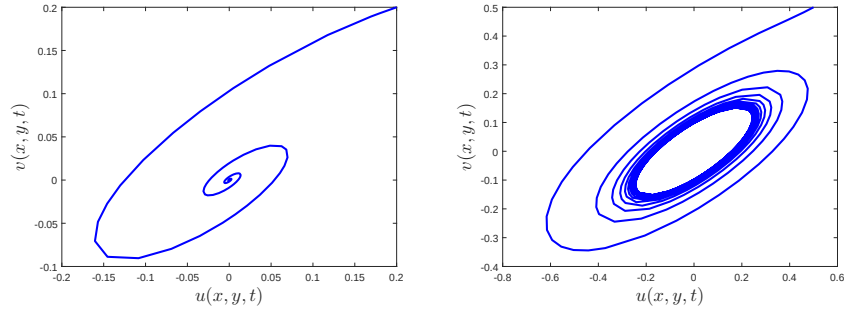

Figure 1. Phase diagrams of system (1.2) with $\tau = 0.02 < \tau_0 = 0.0759$ (see left-hand figure) and $\tau = 0.08 > \tau_0 = 0.0681$ (see right-hand figure), where $c_1 = 2$, $c_2 = 4$, $a_1 = -4$, $a_2 = 2$, $b_1 = 3.6$, $b_2 = 1.2$ and $f_i(\cdot), g_i(\cdot)$ $(i = 1, 2)$ are chosen as $\tanh(\cdot)$.

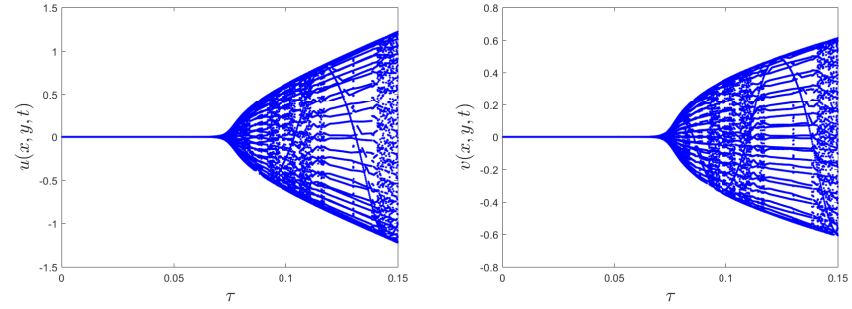

Figure 2. The bifurcation diagram of system (1.2) with respect to the delay $\tau \in [0, 0.15]$.

2.2. Turing instability analysis

In this section, we study the conditions of Turing instability in system (1.2) based on the pattern dynamics theory proposed by Turing [22].

In reality, both leakage delay τ_1 and synaptic transmission delay τ_2 are relatively small. For such a small delay, we develop $u(t-\tau)$, $v(t-\tau)$ into power series of τ

and only remain the first order terms

$$u(x,y,t-\tau)=u(x,y,t)-\tau\frac{\partial u(x,y,t)}{\partial t},\quad v(x,y,t-\tau)=v(x,y,t)-\tau\frac{\partial v(x,y,t)}{\partial t}. \tag{2.8}$$

Substituting (2.8) into (2.1), we obtain that

$$\begin{cases}(1-c_1\tau)\dfrac{\partial u(x,y,t)}{\partial t}+\phi_1\tau\dfrac{\partial v(x,y,t)}{\partial t}=&d_1\Delta u(x,y,t)-c_1u(x,y,t)+\phi_1v(x,y,t)\\ &+\varphi_1u(x,y,t),\\ (1-c_2\tau)\dfrac{\partial v(x,y,t)}{\partial t}+\phi_2\tau\dfrac{\partial u(x,y,t)}{\partial t}=&d_2\Delta v(x,y,t)-c_2v(x,y,t)+\phi_2u(x,y,t)\\ &+\varphi_2v(x,y,t).\end{cases}$$

By direct calculation, it follows that

$$\begin{cases}\dfrac{\partial u(x,y,t)}{\partial t}=&D_{11}(\tau)\Delta u(x,y,t)+D_{12}(\tau)\Delta v(x,y,t)+A_1(\tau)u(x,y,t)\\ &+B_1(\tau)v(x,y,t),\\ \dfrac{\partial v(x,y,t)}{\partial t}=&D_{21}(\tau)\Delta u(x,y,t)+D_{22}(\tau)\Delta v(x,y,t)+A_2(\tau)u(x,y,t)\\ &+B_2(\tau)v(x,y,t),\end{cases} \tag{2.9}$$

where

$$\begin{aligned}&D_{11}(\tau)=\frac{d_1(1-c_2\tau)}{(1-c_1\tau)(1-c_2\tau)-\phi_1\phi_2\tau^2},\quad D_{12}(\tau)=-\frac{\phi_1d_2\tau}{(1-c_1\tau)(1-c_2\tau)-\phi_1\phi_2\tau^2},\\ &A_1(\tau)=\frac{(\varphi_1-c_1)(1-c_2\tau)-\phi_1\phi_2\tau}{(1-c_1\tau)(1-c_2\tau)-\phi_1\phi_2\tau^2},\quad B_1(\tau)=\frac{\phi_1(1-c_2\tau)+\phi_1\tau(c_2-\varphi_2)}{(1-c_1\tau)(1-c_2\tau)-\phi_1\phi_2\tau^2},\\ &D_{21}(\tau)=\frac{d_1-D_{11}(\tau)(1-c_1\tau)}{\phi_1\tau},\qquad D_{22}(\tau)=-\frac{D_{12}(\tau)(1-c_1\tau)}{\phi_1\tau},\\ &A_2(\tau)=\frac{\varphi_1-c_1-A_1(\tau)(1-c_1\tau)}{\phi_1\tau},\qquad B_2(\tau)=\frac{\phi_1-B_1(\tau)(1-c_1\tau)}{\phi_1\tau}.\end{aligned}$$

Thus, we only need to investigate system (2.9), which can be regard as a cross-diffusion model. Linearizing system (2.9) at E_0, we have

$$\lambda^2-\mathrm{tr}_k(J)\lambda+\det_k(J)=0,$$

where

$$J=\begin{pmatrix}A_1(\tau)-D_{11}(\tau)k^2 & B_1(\tau)-D_{12}(\tau)k^2\\ A_2(\tau)-D_{21}(\tau)k^2 & B_2(\tau)-D_{22}(\tau)k^2\end{pmatrix}.$$

The eigenvalues λ_k are calculated as

$$\lambda_k=\frac{\mathrm{tr}_k(J)\pm\sqrt{\mathrm{tr}_k^2(J)-4\det_k(J)}}{2},$$

where

$$\begin{aligned}\mathrm{tr}_k(J) =& A_1(\tau)+B_2(\tau)-(D_{11}(\tau)+D_{22}(\tau))\,k^2,\\ \det_k(J) =& (D_{11}(\tau)D_{22}(\tau)-D_{12}(\tau)D_{21}(\tau))\,k^4\\ &-(A_1(\tau)D_{22}(\tau)+B_2(\tau)D_{11}(\tau)-A_2(\tau)D_{12}(\tau)-B_1(\tau)D_{21}(\tau))\,k^2\\ &+A_1(\tau)B_2(\tau)-A_2(\tau)B_1(\tau).\end{aligned} \tag{2.10}$$

The unbalanced changes of phases, corresponding to Turing branches, are the transitions of system (2.9) from the uniform state to the oscillatory state. After the process, the formed patterns are called Turing patterns. From (2.10), we can obtain the necessary conditions for causing Turing instability:

$$\begin{aligned}&(\mathbf{H2})\quad \mathrm{tr}_0(J) = A_1(\tau)+B_2(\tau)<0,\\ &(\mathbf{H3})\quad \det_0(J) = A_1(\tau)B_2(\tau)-A_2(\tau)B_1(\tau)>0,\\ &(\mathbf{H4})\quad \det_k(J) = (D_{11}(\tau)D_{22}(\tau)-D_{12}(\tau)D_{21}(\tau))\,k^4\\ &\qquad\qquad -(A_1(\tau)D_{22}(\tau)+B_2(\tau)D_{11}(\tau)-A_2(\tau)D_{12}(\tau)-B_1(\tau)D_{21}(\tau))\,k^2\\ &\qquad\qquad +A_1(\tau)B_2(\tau)-A_2(\tau)B_1(\tau)<0.\end{aligned}$$

(**H2**)-(**H4**) indicate that the system is unstable for some perturbations to the wave number k. Thus we have $\det_k(J)=0$ at the critical value. That is to say, Turing bifurcation occurs when $\mathrm{Im}(\lambda_k)=0$, $\mathrm{Re}(\lambda_k)=0$, at $k=k_T\neq 0$. The critical value of the Turing bifurcation parameter τ_T is determined by the following equation

$$\begin{aligned}&(A_1(\tau_T)D_{22}(\tau_T)+B_2(\tau_T)D_{11}(\tau_T)-A_2(\tau_T)D_{12}(\tau_T)-B_1(\tau_T)D_{21}(\tau_T))^2\\ &-4\,(A_1(\tau_T)B_2(\tau_T)-A_2(\tau_T)B_1(\tau_T))(D_{11}(\tau_T)D_{22}(\tau_T)-D_{12}(\tau_T)D_{21}(\tau_T))=0.\end{aligned}$$

When Turing patterns come into being, the wave number k_T satisfies

$$k_T^2=\frac{A_1(\tau)D_{22}(\tau)+B_2(\tau)D_{11}(\tau)-A_2(\tau)D_{12}(\tau)-B_1(\tau)D_{21}(\tau)}{2(D_{11}(\tau)D_{22}(\tau)-D_{12}(\tau)D_{21}(\tau))}.$$

Solving $\det_k(J)=0$, we obtain that

$$B_2(\tau,k)=D_{22}(\tau)k^2+\left(B_1(\tau)-D_{12}(\tau)k^2\right)\frac{D_{21}(\tau)k^2-A_2(\tau)}{D_{11}(\tau)k^2-A_1(\tau)}.$$

Letting $B_2(\tau,k)=B_2(\tau,k+1)$ yields

$$\begin{aligned}B_1(\tau,k,k+1)=&\frac{D_{22}(\tau)\left(D_{11}(\tau)k^2-A_1(\tau)\right)\left[D_{11}(\tau)(k+1)^2-A_1(\tau)\right]}{A_1(\tau)D_{21}(\tau)-A_2(\tau)D_{11}(\tau)}\\ &+\frac{A_1(\tau)D_{12}(\tau)D_{21}(\tau)\left[(k+1)^2+k^2\right]}{A_1(\tau)D_{21}(\tau)-A_2(\tau)D_{11}(\tau)}\\ &-\frac{D_{11}(\tau)D_{12}(\tau)D_{21}(\tau)k^2(k+1)^2+A_1(\tau)A_2(\tau)D_{12}(\tau)}{A_1(\tau)D_{21}(\tau)-A_2(\tau)D_{11}(\tau)}.\end{aligned}$$

From above discussions, we can get the following result.

Theorem 2.2. *If (***H2***), (***H3***) and the following conditions hold:*

$$(\mathbf{H5})\quad A_1(\tau)D_{22}(\tau)+B_2(\tau)D_{11}(\tau)-A_2(\tau)D_{12}(\tau)-B_1(\tau)D_{21}(\tau)>0,$$

$$\textbf{(H6)}\quad (A_1(\tau)D_{22}(\tau)+B_2(\tau)D_{11}(\tau)-A_2(\tau)D_{12}(\tau)-B_1(\tau)D_{21}(\tau))^2 - 4(A_1(\tau)B_2(\tau)-A_2(\tau)B_1(\tau))(D_{11}(\tau)D_{22}(\tau)-D_{12}(\tau)D_{21}(\tau))>0,$$

meanwhile, $B_2(\tau)=B_2(\tau,k)$ *and* $B_1(\tau)\in[B_1(\tau,k-1,k),B_1(\tau,k,k+1))$ *in which* $k\subset\mathbb{N}^+$*, then system* (1.2) *will undergoes* $k-$*mode Turing bifurcation.*

According to Theorem 2.2, the conditions of Turing instability are determined by τ due to that all coefficients of system (2.9) are functions with respective to τ. Denote the left hand terms of inequations in conditions (**H2**), (**H3**), (**H5**) and (**H6**) by $h_1(\tau)$, $h_2(\tau)$, $h_3(\tau)$, $h_4(\tau)$, namely, Turing instability occurs when $h_1(\tau)<0$ and $h_2(\tau),h_3(\tau),h_4(\tau)>0$. To further investigate the conditions of Turing instability, we set φ_1 as a free parameter and fix other parameters. The trajectories of $h_1(\tau)$, $h_2(\tau)$, $h_3(\tau)$ and $h_4(\tau)$ with respect to the delay τ are drawn in Fig. 3. From Fig. 3(a), it is easy to find that Turing instability may happen at $\tau\in[0,0.079]$ (marked by the small yellow region in Fig. 3(a)). When φ_1 varies from 3.6 to 3.1, we observe in Fig. 3(b) that Turing instability cannot come up in system (1.2).

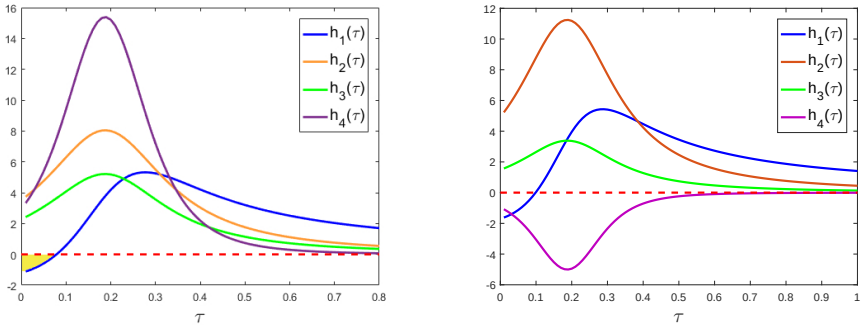

(a) (b)

Figure 3. The trajectories of $h_1(\tau)$, $h_2(\tau)$, $h_3(\tau)$ and $h_4(\tau)$ with respect to the delay τ, where $d_1=0.1$, $d_2=1.6$, $c_1=2$, $c_2=4$, $\phi_1=-4$, $\phi_2=2$, $\varphi_1=3.6$, $\varphi_2=1.2$ (Fig. 3(a)) and $d_1=0.1$, $d_2=1.6$, $c1=2$, $c_2=4$, $\phi_1=-4$, $\phi_2=2$, $\varphi_1=3.1$, $\varphi_2=1.2$ (Fig. 3(b)). $f_i(\cdot),g_i(\cdot)$ $(i=1,2)$ are chosen as $\tanh(\cdot)$.

3. Amplitude equations

In this section, based on the multiple-scale analysis method, we derive the amplitude equations near the instability threshold, which help us determine the different Turing patterns. From [17], the basic state is unstable only in regard to perturbations with wave numbers close to the critical value k_T. For more details concerning the multiple-scale analysis method, please refer to [7, 28, 29, 31].

First, we develop $u(t-\tau)$, $v(t-\tau)$ into power series of τ and only remain the first order terms, in which reaction-diffusion terms are also considered. Then, system

(1.2) is transformed into

$$\begin{cases} \dfrac{\partial u(x,y,t)}{\partial t} = d_1\Delta u(x,y,t) - c_1\tilde{u}(x,y,t) + a_1 f_1(\tilde{v}(x,y,t)) + b_1 g_1(u(x,y,t)), \\ \dfrac{\partial v(x,y,t)}{\partial t} = d_2\Delta v(x,y,t) - c_2\tilde{v}(x,y,t) + a_2 f_2(\tilde{u}(x,y,t)) + b_2 g_2(v(x,y,t)), \\ \dfrac{\partial \tilde{u}(x,y,t)}{\partial t} = \Delta\tilde{u}(x,y,t) + \dfrac{1}{\tau}(u(x,y,t) - \tilde{u}(x,y,t)), \\ \dfrac{\partial \tilde{v}(x,y,t)}{\partial t} = \Delta\tilde{v}(x,y,t) + \dfrac{1}{\tau}(v(x,y,t) - \tilde{v}(x,y,t)), \end{cases} \tag{3.1}$$

where $\tilde{u}(x,y,t) = u(x,y,t-\tau)$, $\tilde{v}(x,y,t) = v(x,y,t-\tau)$. For simplicity, we set $f_j(\cdot)$, $g_j(\cdot)$ $(j = 1, 2)$ as $\tanh(\cdot)$. According to Taylor series expansion, system (3.1) can be rewritten as

$$\begin{cases} \dfrac{\partial u(x,y,t)}{\partial t} =& d_1\Delta u(x,y,t) - c_1\tilde{u}(x,y,t) + a_1\tilde{v}(x,y,t) + b_1 u(x,y,t) \\ & - \dfrac{1}{3}a_1\tilde{v}^3(x,y,t) - \dfrac{1}{3}b_1 u^3(x,y,t), \\ \dfrac{\partial v(x,y,t)}{\partial t} =& d_2\Delta v(x,y,t) - c_2\tilde{v}(x,y,t) + a_2\tilde{u}(x,y,t) + b_2 v(x,y,t) \\ & - \dfrac{1}{3}a_2\tilde{u}^3(x,y,t) - \dfrac{1}{3}b_2 v^3(x,y,t), \\ \dfrac{\partial \tilde{u}(x,y,t)}{\partial t} =& \Delta\tilde{u}(x,y,t) + \dfrac{1}{\tau}(u(x,y,t) - \tilde{u}(x,y,t)), \\ \dfrac{\partial \tilde{v}(x,y,t)}{\partial t} =& \Delta\tilde{v}(x,y,t) + \dfrac{1}{\tau}(v(x,y,t) - \tilde{v}(x,y,t)). \end{cases} \tag{3.2}$$

The Turing patterns of system (3.2) can be described by the modulus that consists of three wave vectors, namely, k_1, k_2 and k_3, which intersect at 120°. The solutions of system (3.2) near the bifurcation threshold can be expanded to

$$P = \begin{pmatrix} u \\ v \\ \tilde{u} \\ \tilde{v} \end{pmatrix} = \sum_{i=1}^{3} \begin{pmatrix} A_j^u \\ A_j^v \\ A_j^{\tilde{u}} \\ A_j^{\tilde{v}} \end{pmatrix} e^{\mathrm{i}k_j r} + \text{c.c.}, \quad j = 1, 2, 3, \tag{3.3}$$

where c.c. stands for the complex conjugate. Then, system (3.2) can be converted to the following system

$$\frac{\partial P}{\partial t} = LP + N, \tag{3.4}$$

where

$$L = \begin{pmatrix} d_1\Delta + b_1 & 0 & -c_1 & a_1 \\ 0 & d_2\Delta + b_2 & a_2 & -c_2 \\ \frac{1}{\tau} & 0 & \Delta - \frac{1}{\tau} & 0 \\ 0 & \frac{1}{\tau} & 0 & \Delta - \frac{1}{\tau} \end{pmatrix}, N = \begin{pmatrix} -\frac{1}{3}b_1 u^3(x,y,t) - \frac{1}{3}a_1\tilde{v}^3(x,y,t) \\ -\frac{1}{3}b_2 v^3(x,y,t) - \frac{1}{3}a_2\tilde{u}^3(x,y,t) \\ 0 \\ 0 \end{pmatrix}.$$

For system (3.4), we need only to analyze the behavior of the controlled parameter τ which is close to the onset τ_T. With this method, we can expand τ in the following term

$$\tau_T - \tau = \varepsilon\tau_{1T} + \varepsilon^2\tau_{2T} + \varepsilon^3\tau_{3T} + o\left(\varepsilon^4\right), \tag{3.5}$$

where ε is a small parameter. Expanding the variable P and the nonlinear term N according to this small parameter, we have the following results

$$\begin{aligned} P &= \begin{pmatrix} u \\ v \\ \tilde{u} \\ \tilde{v} \end{pmatrix} = \varepsilon \begin{pmatrix} u_1 \\ v_1 \\ \tilde{u}_1 \\ \tilde{v}_1 \end{pmatrix} + \varepsilon^2 \begin{pmatrix} u_2 \\ v_2 \\ \tilde{u}_2 \\ \tilde{v}_2 \end{pmatrix} + \varepsilon^3 \begin{pmatrix} u_3 \\ v_3 \\ \tilde{u}_3 \\ \tilde{v}_3 \end{pmatrix} + o(\varepsilon^4), \\ N &= \varepsilon^3 h_3 + o(\varepsilon^4), \end{aligned} \tag{3.6}$$

where h_3 corresponds to the third order of ε in the expansion of the nonlinear operator. Next, L can be expanded as follows

$$L = L_T + (\tau_T - \tau)M, \tag{3.7}$$

where

$$L_T = \begin{pmatrix} d_1\Delta + b_1 & 0 & -c_1 & a_1 \\ 0 & d_2\Delta + b_2 & a_2 & -c_2 \\ \frac{1}{\tau_T} & 0 & \Delta - \frac{1}{\tau_T} & 0 \\ 0 & \frac{1}{\tau_T} & 0 & \Delta - \frac{1}{\tau_T} \end{pmatrix}, \quad M = \begin{pmatrix} 0 & 0 & 0 & 0 \\ 0 & 0 & 0 & 0 \\ \frac{1}{\tau\tau_T} & 0 & -\frac{1}{\tau\tau_T} & 0 \\ 0 & \frac{1}{\tau\tau_T} & 0 & -\frac{1}{\tau\tau_T} \end{pmatrix}.$$

The essence of the multiple-scale analysis method is separating the dynamical behaviors of system (3.1) according to different time scale or spatial scale. In this section, we just need to separate the time scale for system (3.4) (i.e. $T_0 = t$, $T_1 = \varepsilon t$, $T_2 = \varepsilon^2 t$). Each time scale T_j $(j = 0, 1, 2)$ can be considered as an independent variable, namely, T_j corresponds to the dynamical behaviors of the variables whose scales are ε^{-j}. Thus the derivative with respect to time converts to the following term

$$\frac{\partial}{\partial t} = \frac{\partial}{\partial T_0} + \varepsilon\frac{\partial}{\partial T_1} + \varepsilon^2\frac{\partial}{\partial T_2} + o(\varepsilon^3).$$

The bases of solution (3.3) have nothing to do with the time, while the amplitude A is a variable that changes slowly. For system (3.4), we consider the following result

$$\frac{\partial A}{\partial t} = \varepsilon\frac{\partial A}{\partial T_1} + \varepsilon^2\frac{\partial A}{\partial T_2} + o\left(\varepsilon^3\right). \tag{3.8}$$

Substituting (3.5)-(3.7) into (3.4) and expanding (3.4) according to different orders of ε, we obtain that

$$\varepsilon:\ L_T \begin{pmatrix} u_1 \\ v_1 \\ \tilde{u}_1 \\ \tilde{v}_1 \end{pmatrix} = 0, \quad \varepsilon^2:\ L_T \begin{pmatrix} u_2 \\ v_2 \\ \tilde{u}_2 \\ \tilde{v}_2 \end{pmatrix} = \frac{\partial}{\partial T_1} \begin{pmatrix} u_1 \\ v_1 \\ \tilde{u}_1 \\ \tilde{v}_1 \end{pmatrix} - \tau_{1T} M \begin{pmatrix} u_1 \\ v_1 \\ \tilde{u}_1 \\ \tilde{v}_1 \end{pmatrix},$$

$$\varepsilon^3:\ L_T\begin{pmatrix}u_3\\ v_3\\ \tilde{u}_3\\ \tilde{v}_3\end{pmatrix}=\frac{\partial}{\partial T_1}\begin{pmatrix}u_2\\ v_2\\ \tilde{u}_2\\ \tilde{v}_2\end{pmatrix}+\frac{\partial}{\partial T_2}\begin{pmatrix}u_1\\ v_1\\ \tilde{u}_1\\ \tilde{v}_1\end{pmatrix}-\tau_{1T}M\begin{pmatrix}u_2\\ v_2\\ \tilde{u}_2\\ \tilde{v}_2\end{pmatrix}-\tau_{2T}M\begin{pmatrix}u_1\\ v_1\\ \tilde{u}_1\\ \tilde{v}_1\end{pmatrix}-h_3.$$

For the first order of ε, as L_T is the linear operator of system (3.1) close to the onset, $(u_1, v_1, \tilde{u}_1, \tilde{v}_1)^T$ is the linear combination of the eigenvectors that corresponds to the eigenvalue 0. Solving the first order of ε yields

$$\begin{pmatrix}u_1\\ v_1\\ \tilde{u}_1\\ \tilde{v}_1\end{pmatrix}=\begin{pmatrix}l_1l_2\\ l_1\\ l_2\\ 1\end{pmatrix}\left(W_1e^{\mathrm{i}k_1r}+W_2e^{\mathrm{i}k_2r}+W_3e^{\mathrm{i}k_3r}\right)+\text{c.c.},\tag{3.9}$$

in which

$$l_1=\tau_Tk_T^2+1,\quad l_2=\frac{a_1}{c_1-(b_1-d_1k_T^2)(\tau_Tk_T^2+1)}.$$

Besides, $|k_j|=k_T$ $(j=1,2,3)$ and c.c. denotes the conjugate of the former terms. W_j is the amplitude of the mode $e^{\mathrm{i}k_jr}$ when the system is under the first-order perturbation, while, its form is determined by the perturbational term of the higher order.

For the second order of ε, we have

$$L_T\begin{pmatrix}u_2\\ v_2\\ \tilde{u}_2\\ \tilde{v}_2\end{pmatrix}=\frac{\partial}{\partial T_1}\begin{pmatrix}u_1\\ v_1\\ \tilde{u}_1\\ \tilde{v}_1\end{pmatrix}-\tau_{1T}M\begin{pmatrix}u_1\\ v_1\\ \tilde{u}_1\\ \tilde{v}_1\end{pmatrix}=\begin{pmatrix}F_u\\ F_v\\ F_{\tilde{u}}\\ F_{\tilde{v}}\end{pmatrix}.\tag{3.10}$$

To make sure Eq. (3.10) has nontrivial solutions, according to Fredholm solubility condition, the vector function of the right-hand side of Eq. (3.10) must be orthogonal with the 0 eigenvector of operator L_T^+. Here, L_T^+ is the adjoint operator of the operator L_T. In addition, the 0 eigenvector of L_T^+ is

$$\begin{pmatrix}1 & l_1' & l_2' & l_3'\end{pmatrix}^T\exp(-\mathrm{i}k_jr)+\text{c.c.},\quad j=1,2,3,$$

where

$$l_1'=\frac{c_1+(\tau_Tk_T^2+1)(d_1k_T^2-b_1)}{a_2},\quad l_2'=\tau_T(d_1k_T^2-b_1),$$
$$l_3'=\frac{\tau_T(d_2k_T^2-b_2)\left[c_1+(\tau_Tk_T^2+1)(d_1k_T^2-b_1)\right]}{a_2}.$$

From the orthogonality condition, we obtain that

$$\begin{pmatrix} 1 & l_1' & l_2' & l_3' \end{pmatrix} \begin{pmatrix} F_u^j \\ F_v^j \\ F_{\tilde{u}}^j \\ F_{\tilde{v}}^j \end{pmatrix} = 0, \tag{3.11}$$

where F_u^j, F_v^j, $F_{\tilde{u}}^j$ and $F_{\tilde{v}}^j$ represent the coefficients corresponding to $e^{\mathrm{i}k_j r}$ in F_u, F_v, $F_{\tilde{u}}$ and $F_{\tilde{v}}$, respectively, that is to say,

$$\begin{pmatrix} F_u \\ F_v \\ F_{\tilde{u}} \\ F_{\tilde{v}} \end{pmatrix} = \begin{pmatrix} F_u^1 \\ F_v^1 \\ F_{\tilde{u}}^1 \\ F_{\tilde{v}}^1 \end{pmatrix} e^{\mathrm{i}k_1 r} + \begin{pmatrix} F_u^2 \\ F_v^2 \\ F_{\tilde{u}}^2 \\ F_{\tilde{v}}^2 \end{pmatrix} e^{\mathrm{i}k_2 r} + \begin{pmatrix} F_u^3 \\ F_v^3 \\ F_{\tilde{u}}^3 \\ F_{\tilde{v}}^3 \end{pmatrix} e^{\mathrm{i}k_3 r}.$$

In later analysis, we only investigate $e^{\mathrm{i}k_1 r}$. From (3.9) and (3.11), we have

$$(l_1 l_2 + l_1 l_1' + l_2 l_2' + l_3') \frac{\partial W_1}{\partial T_1} = \frac{\tau_{1T}(l_1 - 1)(l_2 l_2' + l_3')}{\tau \tau_T} W_1. \tag{3.12}$$

Then, substituting (3.9) into (3.10) yields

$$\begin{pmatrix} u_2 \\ v_2 \\ \tilde{u}_2 \\ \tilde{v}_2 \end{pmatrix} = \sum_{i=1}^{3} \begin{pmatrix} U_i \\ V_i \\ \tilde{U}_i \\ \tilde{V}_i \end{pmatrix} e^{ik_i r} + \text{c.c.}, \tag{3.13}$$

in which $U_i = l_1 l_2 \tilde{V}_i$, $V_i = l_1 \tilde{V}_i$, $\tilde{U}_i = l_2 \tilde{V}_i$. For the third order of ε, it follows that

$$\begin{aligned} L_T \begin{pmatrix} u_3 \\ v_3 \\ \tilde{u}_3 \\ \tilde{v}_3 \end{pmatrix} &= \frac{\partial}{\partial T_1} \begin{pmatrix} u_2 \\ v_2 \\ \tilde{u}_2 \\ \tilde{v}_2 \end{pmatrix} + \frac{\partial}{\partial T_2} \begin{pmatrix} u_1 \\ v_1 \\ \tilde{u}_1 \\ \tilde{v}_1 \end{pmatrix} - \tau_{1T} M \begin{pmatrix} u_2 \\ v_2 \\ \tilde{u}_2 \\ \tilde{v}_2 \end{pmatrix} - \tau_{2T} M \begin{pmatrix} u_1 \\ v_1 \\ \tilde{u}_1 \\ \tilde{v}_1 \end{pmatrix} - h_3 \\ &= \begin{pmatrix} H_u \\ H_v \\ H_{\tilde{u}} \\ H_{\tilde{v}} \end{pmatrix}. \end{aligned} \tag{3.14}$$

Similarly, H_u^j, H_v^j, $H_{\tilde{u}}^j$ and $H_{\tilde{v}}^j$ correspond to $e^{\mathrm{i}k_j r}$ in H_u, H_v, $H_{\tilde{u}}$ and $H_{\tilde{v}}$, respectively. Then, we derive that

$$\begin{pmatrix} H_u^1 \\ H_v^1 \\ H_{\tilde{u}}^1 \\ H_{\tilde{v}}^1 \end{pmatrix} = \begin{pmatrix} l_1 l_2 \\ l_1 \\ l_2 \\ 1 \end{pmatrix} \left(\frac{\partial \tilde{V}_1}{\partial T_1} + \frac{\partial W_1}{\partial T_2} \right) - \frac{(l_1 - 1)}{\tau \tau_T} \begin{pmatrix} 0 \\ 0 \\ l_2 \\ 1 \end{pmatrix} \left(\tau_{1T} \tilde{V}_1 + \tau_{2T} W_1 \right) + \begin{pmatrix} G_{11} \left| W_1^2 \right| + G_{12} \left(\left| W_2^2 \right| + \left| W_3^2 \right| \right) \\ G_{21} \left| W_1^2 \right| + G_{22} \left(\left| W_2^2 \right| + \left| W_3^2 \right| \right) \\ 0 \\ 0 \end{pmatrix} W_1,$$

where

$$G_{11} = b_1 l_1^3 l_2^3 + a_1, \quad G_{12} = 2G_{11}, \quad G_{21} = b_2 l_1^3 + a_2 l_2^3, \quad G_{22} = 2G_{21}.$$

According to Fredholm solubility condition, it follows that

$$\begin{aligned} &(l_1 l_2 + l_1 l_1' + l_2 l_2' + l_3') \left(\frac{\partial \tilde{V}_1}{\partial T_1} + \frac{\partial W_1}{\partial T_2} \right) = \frac{(l_1 - 1)(l_2 l_2' + l_3')}{\tau \tau_T} \left(\tau_{1T} \tilde{V}_1 + \tau_{2T} W_1 \right) \\ &- \left[(G_{11} + l_1' G_{21}) \left| W_1^2 \right| + (G_{12} + l_1' G_{22}) \left(\left| W_2^2 \right| + \left| W_3^2 \right| \right) \right] W_1. \end{aligned} \tag{3.15}$$

Let $A_i = A_i^u = l_2 A_i^v = l_1 A_i^{\tilde{u}} = l_1 l_2 A_i^{\tilde{v}}$ be the coefficient of $e^{ik_i r}$, then

$$\begin{pmatrix} A_i^u \\ A_i^v \\ A_i^{\tilde{u}} \\ A_i^{\tilde{v}} \end{pmatrix} = \varepsilon \begin{pmatrix} l_1 l_2 \\ l_1 \\ l_2 \\ 1 \end{pmatrix} W_i + \varepsilon^2 \begin{pmatrix} l_1 l_2 \\ l_1 \\ l_2 \\ 1 \end{pmatrix} \tilde{V}_i + o(\varepsilon^3), \quad i = 1, 2, 3. \tag{3.16}$$

Multiplying (3.12) and (3.15) by ε, ε^2, respectively, meanwhile, using (3.8) and (3.16) to merge the variables, we obtain the amplitude equation corresponding to A_1 as follows

$$\tau_0 \frac{\partial A_1}{\partial t} = \mu A_1 - [g_1 |A_1|^2 + g_2 (|A_2|^2 + |A_3|^2)] A_1, \tag{3.17}$$

where

$$\tau_0 = \frac{\tau (l_1 l_2 + l_1 l_1' + l_2 l_2' + l_3')}{(l_1 - 1)(l_2 l_2' + l_3')}, \quad \mu = \frac{\tau_T - \tau}{\tau_T}, \quad g_1 = \frac{\tau \left(G_{11} + l_1' G_{21} \right)}{(l_1 - 1)(l_2 l_2' + l_3')}, \quad g_2 = 2 g_1.$$

As for other cases, we can get corresponding results by changing subscripts.

4. Turing pattern analysis

In this section, we investigate the stability of amplitude equations and construct different Turing patterns. Denote the amplitudes in Eq. (3.17) as follows

$$A_i = \rho_i e^{\mathrm{i}\phi_i}, \quad i = 1, 2, 3, \tag{4.1}$$

where mode $\rho_i = |A_i|$ and ϕ_i is the corresponding phase angle. Substituting (4.1) into (3.17) and separating the real and imaginary parts yield

$$\begin{cases} \tau_0 \dfrac{\partial \phi}{\partial t} = 0, \\ \tau_0 \dfrac{\partial \rho_1}{\partial t} = \mu\rho_1 - g_1\rho_1^3 - g_2(\rho_2^2 + \rho_3^2)\rho_1, \\ \tau_0 \dfrac{\partial \rho_2}{\partial t} = \mu\rho_2 - g_1\rho_2^3 - g_2(\rho_1^2 + \rho_3^2)\rho_2, \\ \tau_0 \dfrac{\partial \rho_3}{\partial t} = \mu\rho_3 - g_1\rho_3^3 - g_2(\rho_1^2 + \rho_2^2)\rho_3, \end{cases} \tag{4.2}$$

where $\phi = \phi_1 + \phi_2 + \phi_3$. Following the pattern dynamics theory proposed by Turing [22], system (4.2) has four kinds of solutions as follows.

(i) The stationary state $\rho_1 = \rho_2 = \rho_3 = 0$.

The stationary state corresponds to the linear perturbation equation $\tau_0 \frac{\partial \rho_i}{\partial t} = \mu\rho_i$. Thus, the stationary state is stable for $\frac{\mu}{\tau_0} < 0$ and unstable for $\frac{\mu}{\tau_0} > 0$.

(ii) Stripe patterns, determined by

$$\rho_1 = \sqrt{\frac{\mu}{g_1}}, \quad \rho_2 = \rho_3 = 0,$$

exist only when $\mu g_1 > 0$.

Set $\hat{\rho}_1 = \sqrt{\frac{\mu}{g_1}} + \sigma_1$, $\hat{\rho}_2 = \sigma_2$, $\hat{\rho}_3 = \sigma_3$. Linearizing Eq. (4.2) at $(\rho_1, 0, 0)$ yields

$$\frac{\partial}{\partial t}\begin{pmatrix} \sigma_1 \\ \sigma_2 \\ \sigma_3 \end{pmatrix} = \begin{pmatrix} -\frac{2\mu}{\tau_0} & 0 & 0 \\ 0 & \frac{\mu}{\tau_0} & 0 \\ 0 & 0 & \frac{\mu}{\tau_0} \end{pmatrix} \begin{pmatrix} \sigma_1 \\ \sigma_2 \\ \sigma_3 \end{pmatrix}.$$

The characteristic equation follows that

$$\left(\lambda + \frac{2\mu}{\tau_0}\right)\left(\lambda + \frac{\mu}{\tau_0}\right)^2 = 0, \tag{4.3}$$

which has three eigenvalues $-\frac{2\mu}{\tau_0}$, $-\frac{\mu}{\tau_0}$, $-\frac{\mu}{\tau_0}$. Thus, if $\frac{\mu}{\tau_0} > 0$, the stripe patterns are stable.

(iii) Spot patterns, determined by

$$\rho_1 = \rho_2 = \rho_3 = \frac{\sqrt{5g_1\mu}}{5g_1},$$

occur when $\mu g_1 > 0$.

Set $\hat{\rho}_1 = \frac{\sqrt{5g_1\mu}}{5g_1} + \sigma_1$, $\hat{\rho}_2 = \frac{\sqrt{5g_1\mu}}{5g_1} + \sigma_2$, $\hat{\rho}_3 = \frac{\sqrt{5g_1\mu}}{5g_1} + \sigma_3$. Linearizing Eq. (4.2) at (ρ_1, ρ_2, ρ_3) yields

$$\frac{\partial}{\partial t}\begin{pmatrix}\sigma_1\\ \sigma_2\\ \sigma_3\end{pmatrix} = \begin{pmatrix}-\frac{2\mu}{5\tau_0} & -\frac{4\mu}{5\tau_0} & -\frac{4\mu}{5\tau_0}\\ -\frac{4\mu}{5\tau_0} & -\frac{2\mu}{5\tau_0} & -\frac{4\mu}{5\tau_0}\\ -\frac{4\mu}{5\tau_0} & -\frac{4\mu}{5\tau_0} & -\frac{2\mu}{5\tau_0}\end{pmatrix}\begin{pmatrix}\sigma_1\\ \sigma_2\\ \sigma_3\end{pmatrix}.$$

The characteristic equation follows that

$$\left(\lambda + \frac{2\mu}{\tau_0}\right)\left(\lambda - \frac{2\mu}{5\tau_0}\right)^2 = 0, \tag{4.4}$$

which has three eigenvalues $-\frac{2\mu}{\tau_0}$, $\frac{2\mu}{5\tau_0}$, $\frac{2\mu}{5\tau_0}$. If $\frac{\mu}{\tau_0} > 0$ or $\frac{\mu}{\tau_0} < 0$, Eq. (4.4) always has positive eigenvalues, then the spot patterns are unstable.

(iv) The mixed patterns, determined by

$$\rho_1 = 0, \quad \rho_2 = \rho_3 = \sqrt{\frac{\mu}{3g_1}},$$

are always unstable.

Remark 4.1. Above discussions imply that Turing patterns of system (1.2) mainly consist of stripe patterns and spot patterns. But, only stripe patterns can keep stable under some circumstances, namely, $\mu g_1 > 0$ and $\frac{\mu}{\tau_0} > 0$.

5. Numerical simulations

Numerical algorithms for reaction-diffusion systems are often complicated, which need tedious MATLAB programming. In [6], Garvie proposed a semi-implicit (in time) finite-difference scheme to approximate the solutions of reaction-diffusion systems. The semi-implicit method means this algorithm involves approximations at the current time level t_n and at the previous time level t_{n-1}. Finally, the algorithm leads to a sparse, banded and linear system of algebraic equations. In this section, to obtain the numerical solutions of system (1.2), we improve the algorithm of Garvie [6] by introducing delay terms into its iterative processes.

System (1.2) is simulated numerically in a $L \times L$ ($L = 50$) two-dimensional square region. We assume that nothing enters this system and nothing exits this system. Thus, we will introduce zero-flux boundary conditions. Time step Δ_t and space step Δ_h are set as 0.005 and 0.25, respectively, which needs large computation but ensures the accuracy of numerical simulations. Diffusion coefficients (d_1, d_2) are chosen as $(0.1, 1.6)$. Besides, $c_1 = 2$, $c_2 = 4$, $a_1 = -4$, $a_2 = 2$. b_1 and b_2 are chosen as free parameters. Let $\tau = n_\tau \Delta_t$ and $t_n = n\Delta_t$.

First, we denote $\hat{f}_i$ and $\hat{g}_i$ $(i = 1, 2)$ as the discrete functions corresponding to f_i and g_i, respectively. Discretize system (1.2) as follows

$$\begin{cases}\dfrac{\partial u_{i,j}(n)}{\partial t} = d_1 \Delta u_{i,j}(n) - c_1 u_{i,j}(n - n_\tau) + a_1 \hat{f}_1(v_{i,j}(n - n_\tau)) + b_1 \hat{g}_1(u_{i,j}(n)),\\ \dfrac{\partial v_{i,j}(n)}{\partial t} = d_2 \Delta v_{i,j}(n) - c_2 v_{i,j}(n - n_\tau) + a_2 \hat{f}_2(u_{i,j}(n - n_\tau)) + b_2 \hat{g}_2(v_{i,j}(n)),\end{cases} \tag{5.1}$$

where $i, j = 0, \cdots, L/\Delta_h$. Denote

$$\mathcal{H}_1(n) = -c_1 u_{i,j}(n - n_\tau) + a_1 \hat{f}_1(v_{i,j}(n - n_\tau)) + b_1 \hat{g}_1(u_{i,j}(n)),$$
$$\mathcal{H}_2(n) = -c_2 v_{i,j}(n - n_\tau) + a_2 \hat{f}_2(u_{i,j}(n - n_\tau)) + b_2 \hat{g}_2(v_{i,j}(n)).$$

Finally, we obtain that

$$\begin{pmatrix} B_1 & 0 \\ 0 & B_2 \end{pmatrix} \begin{pmatrix} u_{i,j}(n+1) \\ v_{i,j}(n+1) \end{pmatrix} = \begin{pmatrix} u_{i,j}(n) + \Delta t \mathcal{H}_1(n) \\ v_{i,j}(n) + \Delta t \mathcal{H}_2(n) \end{pmatrix},$$

where the constant matrices B_1 and B_2 can be referred to [6].

Taking parameter values in Fig. 4 into the expressions of μ, τ_0 and g_1, we have $\mu = 0.9940 > 0$, $\tau_0 = 0.0028 > 0$, $g_1 = 0.0921 > 0$. According to the theoretical analysis, there might be both stripe and spot patterns in this circumstance, but only the stripe patterns are stable. As we can observe in Fig. 4, it forms mixed patterns at first, mainly including spot patterns. As time T increases from 0 to 200, spot patterns fade away and stripe patterns prevail through all the domain.

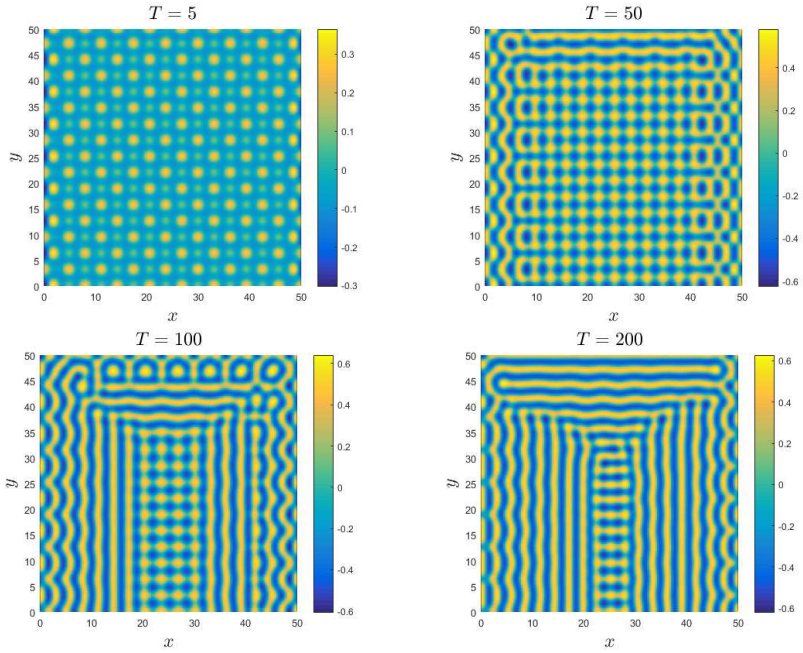

Figure 4. Snapshots of contour pictures of the time evolution of $u(x, y, t)$ at time $T = 5, 50, 100, 200$, respectively, with parameter values $\tau = 0.01$, $d_1 = 0.1$, $d_2 = 1.6$, $c_1 = 2$, $c_2 = 4$, $a_1 = -4$, $a_2 = 2$ $b_1 = 3.4$, $b_2 = 1.2$ and initial condition $u_0 = v_0 = \sin(x)\cos(y) + \xi(x, y)$ in which $\xi(x, y)$ is a stochastic process with respect to the spatial variable (x, y).

The stability of the homogeneous steady state E_0 is the precondition for the occurrence of Turing instability. Usually, larger leakage delay and synaptic transmission delay may give rise to Hopf bifurcation and weaken the stability performance of E_0, which is illustrated in Section 2.1. Naturally rises a question that whether leakage delay and synaptic transmission delay have some effects on the conditions of Turing instability. In Fig. 5, choose (b_1, b_2) as free parameters and project the

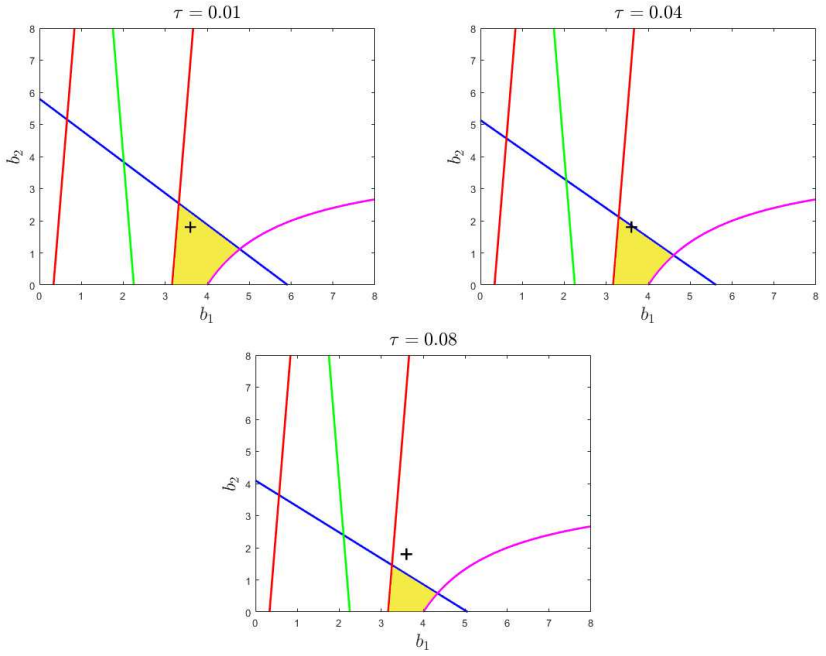

Figure 5. The bifurcation diagram of the parameters b_1 and b_2 with $\tau = 0.01, 0.04, 0.08$, respectively, where $d_1 = 0.1$, $d_2 = 1.6$, $c_1 = 2$, $c_2 = 4$, $a_1 = -4$, $a_2 = 2$. The position of the '+' is $(3.6, 1.8)$.

parameter set (consists of d_1, d_2, c_1, c_2, a_1, a_2, b_1 and b_2) into a two-dimensional space with respect to (b_1, b_2). When (b_1, b_2) stays in the yellow regions in Fig. 5, Turing instability occurs in system (1.2). As τ increases from 0.01 to 0.08, the yellow region shrinks gradually.

Besides, we select a position of the mark '+', which stays in the yellow region of the first figure ($\tau = 0.01$) in Fig. 5 but stays outside the yellow region of the last figure ($\tau = 0.08$). In Fig. 6, its parameter values correspond with the mark '+' of the first figure ($\tau = 0.01$) in Fig. 5, and we observe that Turing patterns with respect to $u(x, y, t)$ form gradually and finally keep their shape. But, once altering τ from 0.01 to 0.08 , as we can see in Fig. 7, Turing patterns with respect to $u(x, y, t)$ always change, which implies that under this condition, system (1.2) cannot form stable patterns, namely, the stability performance of Turing patterns is weakened by leakage delay and synaptic transmission delay.

6. Conclusion

In this paper, we proposed a reaction-diffusion neural network with leakage delay. The existence of Hopf bifurcation was investigated by analyzing characteristic equations, while the conditions of Turing instability were derived following the pattern dynamics theory proposed by Turing [22]. Based on the multiple-scale analysis, we derived the amplitude equations of system (1.2), which help us determine the selection and competition of Turing patterns. In actual neural network circuits, both leakage delay and synaptic transmission delay are relatively small and the error of our theoretical analysis is little. Numerical simulations illustrate our theoretical

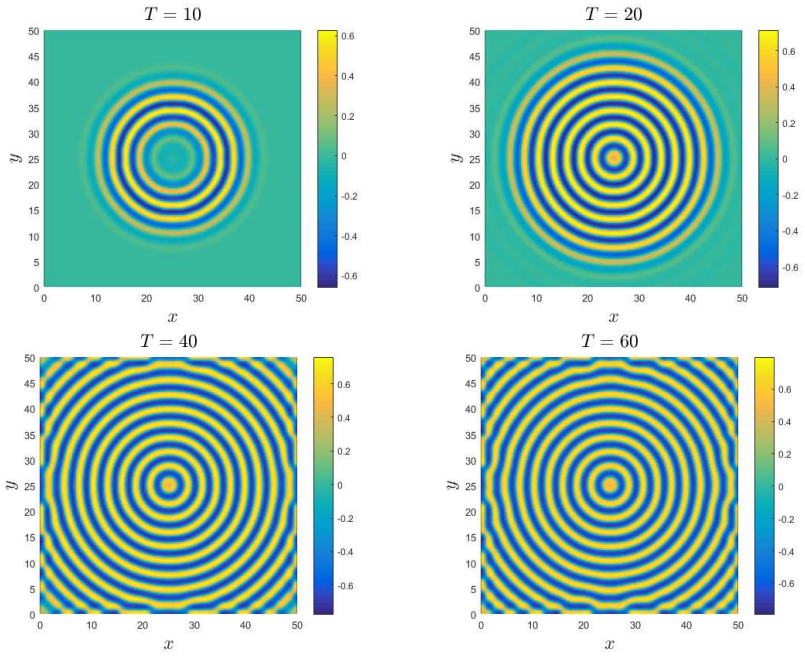

Figure 6. Snapshots of contour pictures of the time evolution of $u(x, y, t)$ at time $T = 10, 20, 40, 60$, respectively, with parameter values $\tau = 0.01$, $d_1 = 0.1$, $d_2 = 1.6$, $c_1 = 2$, $c_2 = 4$, $a_1 = -4$, $a_2 = 2$, $b_1 = 3.6$, $b_2 = 1.8$ and initial condition $u_0 = v_0 = (x - 25)^2 + (y - 25)^2 < 100$.

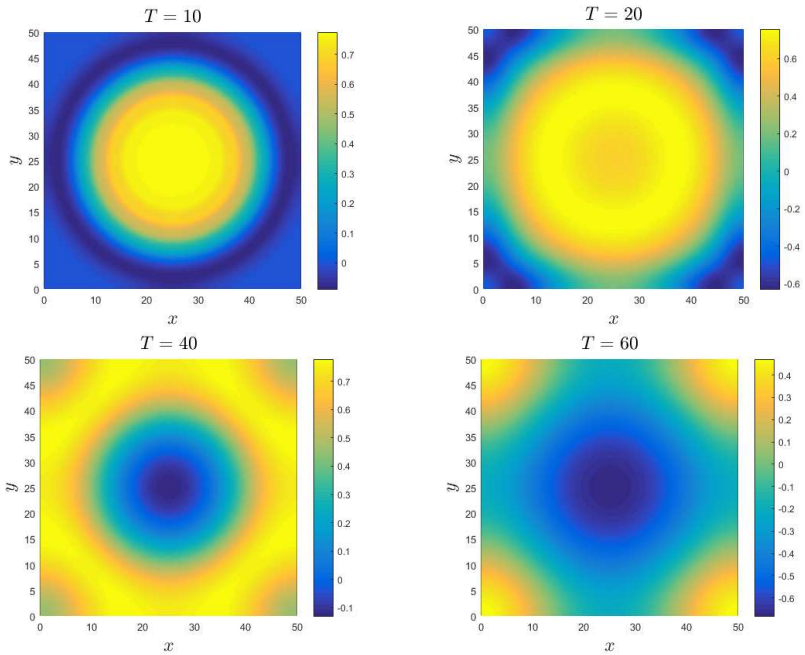

Figure 7. Snapshots of contour pictures of the time evolution of $u(x, y, t)$ at time $T = 10, 20, 40, 60$, respectively, where $\tau = 0.08$ and other parameter values are similar to those in Fig. 6.

analysis and reveal the impact of leakage delay and synaptic transmission delay on the dynamical behaviors of system (1.2). As time delays in system (1.2) increase, the conditions of Turing instability are changed, namely, the former stable Turing patterns may become unstable.

Pattern dynamics in neural networks with diffusion has been investigated in [2, 28], but previous research does not consider leakage delay or synaptic transmission delay. In our study, we illustrate the impact of leakage delay on spatial and temporal dynamics in system (1.2) and obtain meaningful results. Recently, the experimental study indicates that fractional calculus can depict the memory and hereditary attributes of neural networks more accurately. In our further work, we will introduce both diffusion and fractional derivative into reaction-diffusion neural networks with leakage delay.

Acknowledgements. The authors are grateful to the anonymous referees for their useful suggestions which improve the contents of this article.

References

[1] G. Bao and Z. Zeng, *Analysis and design of associative memories based on recurrent neural network with discontinuous activation functions*, Neurocomputing, 2012, 77(1), 101–107.

[2] L. O. Chua and L. Goraş, *Turing patterns in cellular neural networks*, International Journal of Electronics, 1995, 79(6), 719–736.

[3] T. Deb, A. K. Ghosh and A. Mukherjee, *Singular value decomposition applied to associative memory of Hopfield neural network*, Materials Today: Proceedings, 2018, 5(1), 2222–2228.

[4] K. Gopalsamy, *Leakage delays in BAM*, Journal of Mathathematical Analysis and Applications, 2007, 325(2), 1117–1132.

[5] K. Gopalsamy, *Stability and oscillations in delay differential equations of population dynamics*, Kluwer Academic, Dordrecht, 1992.

[6] M. Garvie, *Finite difference schemes for reaction-diffusion equations modeling predator-prey interactions in MATLAB*, Bulletin of Mathematical Biology, 2007, 69(3), 931–956.

[7] B. Han and Z. Wang, *Turing patterns of a Lotka-Volterra competitive system with nonlocal delay*, International Journal of Bifurcation and Chaos, 2018, 28(7), 1830021.

[8] C. Huang, L. Huang, J. Feng, M. Nai and Y. He, *Hopf bifurcation analysis for a two-neuron network with four delays*, Chaos, Solitons and Fractals, 2007, 34, 795–812.

[9] C. Huang, Y. He, L. Huang and Z. Yuan, *Hopf bifurcation analysis of two neurons with three delays*, Nonlinear Analysis: Real World Applications, 2007, 8(3), 903–921.

[10] C. Huang, Y. Meng, J. Cao, A. Alsaedi and F. Alsaadi, *New bifurcation results for fractional BAM neural network with leakage delay*, Chaos, Solitons and Fractals, 2017, 100, 31–44.

[11] C. Huang and J. Cao, *Impact of leakage delay on bifurcation in high-order fractional BAM neural networks*, Neural Networks, 2018, 98, 223–235.

[12] B. Kosko, *Neural Networks and Fuzzy Systems*, Prentice Hall, New Delhi, 1992.

[13] Z. Lin, D. Ma, J. Meng and L. Chen, *Relative ordering learning in spiking neural network for pattern recognition*, Neurocomputing, 2018, 275, 94–106.

[14] P. Melin and D. Sánchez, *Multi-objective optimization for modular granular neural networks applied to pattern recognition*, Information Sciences, 2017, 460–461, 594–610.

[15] T. Mikołajczyk, K. Nowicki, A. Bustillo and D.Y. Pimenov, *Predicting tool life in turning operations using neural networks and image processing*, Mechanical Systems and Signal Processing, 2018, 104, 503–513.

[16] L. Olien and J. Bélair, *Bifurcations, stability, and monotonicity properties of a delayed neural network model*, Physica D, 1997, 102(3–4), 349–363.

[17] Q. Ouyang, *Patterns Formation in Reaction-diffusion Systems*, Shanghai Science and Technology Education Press, Shanghai, 2000.

[18] R. Sakthivel, P. Vadivel, K. Mathiyalagan, A. Arunkumar and M. Sivachitra, *Design of state estimator for bidirectional associative memory neural networks with leakage delays*, Information Sciences, 2015, 296, 263–274.

[19] Y. Seo and K. Shin, *Hierarchical convolutional neural networks for fashion image classification*, Expert Systems with Applications, 2019, 116, 328–339.

[20] X. Tian and R. Xu, *Hopf bifurcation analysis of a reaction-diffusion neural network with time delay in leakage terms and distributed delays*, Neural Processing Letters, 2016, 43(1), 173–193.

[21] X. Tian, R. Xu and Q. Gan, *Hopf bifurcation analysis of a BAM neural network with multiple time delays and diffusion*, Applied Mathematics and Computation, 2015, 266, 909–926.

[22] A.M. Turing, *The chemical basis of morphogenesis*, Philosophical Transactions of the Royal Society B, 1952, 237(1–2), 37–72.

[23] S. Tyagi, S. Jain, S. Abbas, S. Meherrem and R. Ray, *Time-delay-induced instabilities and Hopf bifurcation analysis in 2-neuron network model with reaction-diffusion term*, Neurocomputing, 2018, 313, 306–315.

[24] Y. Wang, J. Cao, G. Sun and J. Li, *Effect of time delay on pattern dynamics in a spatial epidemic model*, Physica A, 2014, 412, 137–148.

[25] Z. Wu, J. Li and J. Li, *Pattern formations of an epidemic model with Allee effect and time delay*, Chaos, Solitons and Fractals, 2017, 104, 599–606.

[26] J. Yang, L. Wang, Y. Wang and T. Guo, *A novel memristive Hopfield neural network with application in associative memory*, Neurocomputing, 2017, 227, 142–148.

[27] H. Yin and X. Wen, *Pattern formation through temporal fractional derivatives*, Scientific Reports, 2018, 8(1), 5070.

[28] H. Zhao, X. Huang and X. Zhang, *Turing instability and pattern formation of neural networks with reaction-diffusion terms*, Nonlinear Dynamics, 2014, 76, 115–124.

[29] X. Zhang, G. Sun and Z. Jin, *Spatial dynamics in a predator-prey model with Beddington-DeAngelis functional response*, Physical Review E, 2012, 85(2), 021924.

[30] Q. Zheng and J. Shen, *Dynamics and pattern formation in a cancer network with diffusion*, Communications in Nonlinear Science and Numerical Simulation, 2015, 27(1–3), 93–109.

[31] Q. Zheng and J. Shen, *Pattern formation in the FitzHugh-Nagumo model*, Computers and Mathematics with Applications, 2015, 70(5), 1082–1097.